Nuclear Inst, and Methods in Physics Research B xxx (xxxx) xxx–xxx

Contents lists available at ScienceDirect

Nuclear Inst. and Methods in Physics Research B

journal homepage: www.elsevier.com/locate/nimb

Cerium-doped lutetium oxyorthosilicate optical waveguide fabricated by ions irradiation: Modification of surface structures and optical properties

Tie-Jun Wang, Mei Qiao, Jing Zhang, Yong Liu, Peng Liu, Xue-Lin Wang*

School of Physics, Key Laboratory of Particle Physics and Particle Irradiation (MOE), Shandong University, Jinan 250100, PR China

ARTICLE INFO

Keywords:
$Ce:Lu_2SiO_5$
Waveguide
Photoluminescence spectroscopy

ABSTRACT

Ion beam technology has been a popular and established method to modify the optical properties of a large variety of crystal materials. In this study, the influence of C^{3+} ion irradiation at an energy of 6.0 MeV with a fluence of 5.0×10^{14} ions/cm^2 on the optical properties, including waveguide and spectral properties, of $Ce:Lu_2SiO_5$ were investigated. First, the displacement per atom (dpa) and X-ray diffraction (XRD) were used to analyze the change in the lattice structure of the irradiated region. The waveguide properties were studied by the prism coupling and end-facing coupling techniques and discussed in terms of the reflectivity calculation method (RCM). The absorption spectra and Raman spectra were measured to analyze the absorption characteristics and molecular vibration of samples. The photoluminescence spectra before and after irradiation were investigated. The experimental results reveal that the intensity of the emission spectra is enhanced after C^{3+} ion irradiation.

1. Introduction

Cerium-doped lutetium oxyorthosilicate ($Ce:Lu_2SiO_5$ or Ce:LSO), which has a tripartite structure, is regarded as a candidate for excellent scintillators, which are used to detect gamma-rays or X-rays in several types of medical instruments, such as computerized tomography (CT) and positron emission tomography (PET) [1]. Additionally, Ce:LSO, with a density of 7.40 g/cm^3, has an emission spectrum at room temperature (peaked approximately 410 nm), and exhibits a high light yield up to approximately 30,000 ph/MeV [2,3]. With a good assembly of high-density and large effective atomic number, Ce:LSO also has an excellent radiation absorption ability, the fast decay time, which is in the nanosecond scale, and a high energy resolution.

Ion beam technology, as a widely applied technique for material modification, has been successfully used to engineer the properties of various materials. Ion beams offer many more options for the beam conditions (e.g., various ion species and wide ranges of ion energies) to realize on-demand modification with high efficiency.

Improving the scintillation properties of Ce:LSO has far-reaching significance and has been studied only to a limited extent [4,5]. In this work, the optical properties including the waveguide and spectral properties, of C^{3+} ion irradiation at an energy of 6.0 MeV with a fluence of 5.0×10^{14} ions/cm^2 on Ce:LSO were investigated. The fluorescence emission band of the Ce^{3+} ions affected by the C^{3+} ion irradiation was explored by a confocal microscopy, which has been discussed previously [6]. The luminescence enhancement effect, present after C^{3+} ion irradiation, is discussed, and the mechanism is revealed.

2. Experimental details

An optically polished z-cut Ce:LSO crystal with dimensions of $5.0 \times 5.0 \times 0.5$ mm^3 was subjected to 6.0 MeV C^{3+} ions with a fluence of 5.0×10^{14} ions/cm^2 utilizing a 2×1.7 MV tandem accelerator at Peking University at room temperature. To minimize channeling effects, the C-ion beam was rastered over the crystal surface at 7° off-surface normal. To describe the mechanism of ion irradiation on Ce:LSO crystal, the SRIM 2013 full-cascade simulation code was used to calculate the dpa.

The C^{3+} ion irradiated cross-section along with an accurate size measurement of the Ce:LSO crystals were observed by a microscope (Axio Imager, Carl Zeiss) and taken using transmitted polarized light. The XRD spectra were performed using Cu $K_{\alpha 1}$ line ($\lambda = 0.15406$ nm) radiation on a Bruker D8 Advance diffractometer. For the waveguide performance at a wavelength of 632.8 nm of Ce:LSO crystals, the dark-mode spectra and optical near-intensity profiles of the TM_0 mode were measured and carried out by the m-line technique via a prism coupler and end-face coupling measurement technique. From the dark-mode spectra, according to the reflectivity method (RCM), the refractive index profile was rebuilt; then the near-intensity profiles were simulated by FD-BPM according to the refractive index profile.

The spectral properties of non-irradiated and irradiated samples were characterized utilizing absorption spectra, micro-Raman spectra,

* Corresponding author.
E-mail address: xuelinwang@sdu.edu.cn (X.-L. Wang).

https://doi.org/10.1016/j.nimb.2018.05.012
Received 19 July 2017; Received in revised form 27 February 2018; Accepted 9 May 2018

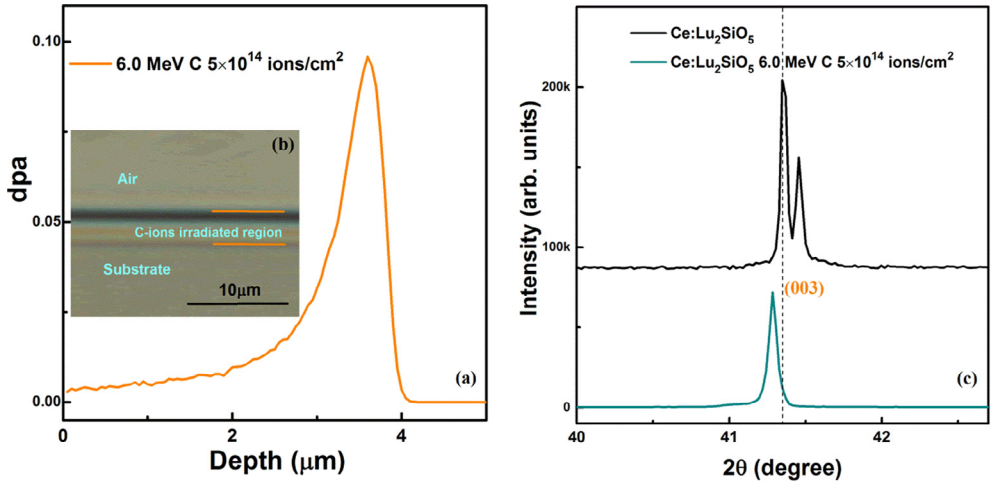

Fig. 1. (a) Simulated dpa profile calculated by SRIM code; (b) metallographic microscopy photograph of the irradiated cross-section of a Ce:LSO sample (c) XRD spectra of un-irradiated and irradiated samples.

and photoluminescence spectra. The absorption spectra of non-irradiated and irradiated samples were recorded using a Jasco U570 spectrophotometer. The micro-Raman spectra at the end face of C^{3+} the irradiated Ce:LSO with different probing locations were performed by a HR800 horiba/Jobin Yvon spectrometer; the laser source of the micro-Raman spectra was 632.8 nm in our experiments. The PL spectra were measured by a Jobin-Yvon iHR320 monochromator; the excitation laser source was d 325 nm.

3. Results and discussion

SRIM code [7] is used to simulate the dpa profile to explore the damage to the crystal structure in the near-surface area in Fig. 1(a). From the figure, it can be seen that the dpa reaches it maximum value of 0.096 at a depth of 3.60 μm after C^{3+} ion irradiation. Fig. 1(b) shows a photograph of the polished cross-section edge of an irradiated sample taken by metallographic microscopy with transmitted light, which visually shows the degree of damage of the near-surface damage region. We found the thickness of the damaged region to be approximately 3.60 μm in the metallographic specimen, which agreed very well with the damage peak of the dpa profile. To further investigate changes to the crystal structure of Ce:LSO samples induced by C^{3+} ion irradiation, the measured XRD patterns are shown in Fig. 1(c). From the figure, it can be seen that the diffraction peak of the non-irradiated sample is approximately about $2\theta = 41.3846^{\circ}$ (corresponding to the reflections from the (0 0 3) crystal planes), while after C^{3+} ion irradiation there is an obvious left-shift to $2\theta = 41.2838^{\circ}$. From Bragg's law, we conclude that the interplanar spacings of non-irradiated and carbon ion irradiated samples are $d_1 = 6.540$ Å and $d_2 = 6.555$ Å, respectively, which means that ion irradiation induced a 0.23% change of the interplanar spacing in the near-surface region. The reason for the change is that the ion irradiation process induces a deformation in lattice structure, and the remnant stress increases the lattice constant of the irradiated region.

The structural change has been investigated and shown in Fig. 1; the waveguides properties were studied and are displayed in Fig. 2. Prism-coupling and end-face coupling methods were used to characterize the properties of the Ce:LSO crystal waveguide at a wavelength of 632.8 nm in the visible band. Fig. 2(a) is the measured dark-mode-line spectra with TM polarized light, which shows the relative intensity of light reflected from a prism versus the effective refractive index of the waveguide. The refractive index of Ce:LSO substrate is $n_{sub} = 1.7968$, which is marked by a dashed line in the figure. In the prism-coupling process, the laser beam can be coupled into the waveguide region, resulting in a dip in the dark-mode spectra; thus, we suppose three guiding modes were formed in this waveguide. From the figure, it is

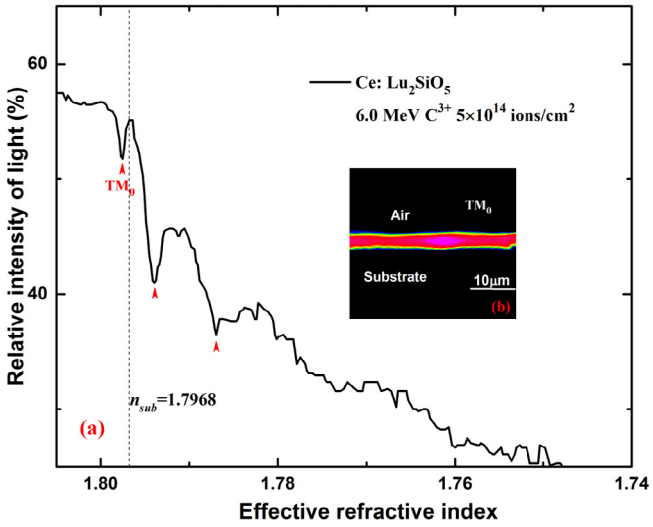

Fig. 2. (a) Measured dark-mode spectra of a Ce:LSO waveguide; (b) near-field light intensity of a waveguide captured by a CCD camera.

obvious that the refractive index of the surface ($n_{sur} = 1.8001$) is higher than that of the substrate, meaning a typical "well" + "barrier" type waveguide was formed in the sample. To ensure the existence of the guiding mode in the waveguide, the end-face coupling method was carried out to collect the near-field light intensity of the waveguide. The 632.8 nm laser was coupled into one end-face of the waveguide by a lens and collected by a lens on another end-face, then captured by a CCD camera. The near-field light intensity shown in Fig. 2(b) proves that the laser beam can be confined well in the waveguide.

We reconstruct the refractive index profile (RIP) of the TM_0 mode at 632.8 nm based on the dark-mode spectra by the RCM code [8], as shown in Fig. 3(a). The RIP of the waveguide is assumed to be a combination of two partial-Gaussian curves. It presents the refractive index of the "well" + "barrier" type waveguide in the near-surface area. The RIP shows the refractive index of the near-surface area is increased compared to that of the substrate and is then followed by a sharp decrease of the refractive index. The decreased area is in accordance with the dpa peak, the reason being that irradiated C^{3+} ions stopped at end of the ion trace, the induced defects decreased the crystal's density, the volume expanded, and a low refractive index barrier region was formed. Based on the RIP, the finite-difference beam propagation method (FD-BPM) [9] was used to simulate the light propagation in the

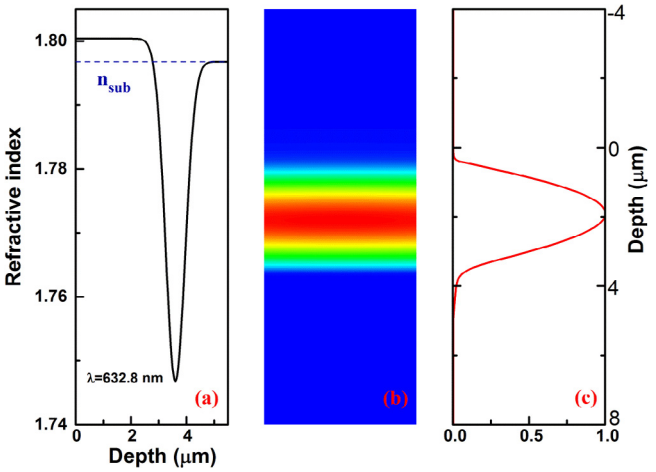

Fig. 3. (a) Calculated RIP of an irradiated sample based on dark-mode spectra; (b) simulated light propagation in the planar waveguide based on the RIP; (c) simulated light intensity distribution versus depth of waveguide.

planar waveguide, as shown the result in Fig. 3(b), and Fig. 3(c) shows the simulated light intensity distribution versus depth. Compared with the measured near-field light intensity, the simulated result agrees well with the experiment, and the simulated RIP is reasonable.

To explore the light absorption characteristics before and after ion irradiation of Ce:LSO, Fig. 4 shows the extinction spectrum of Ce:LSO crystal at wavelengths from 200 to 1000 nm before and after C^{3+} ion irradiation at room temperature. The peaks at 262 nm, 295 nm, and 358 nm were observed and caused by 4f-5d transitions in the Ce^{3+} ions. After C^{3+} ion irradiation, the extinction coefficient of Ce:LSO has obviously increased, and the reason is that the irradiated C^{3+} ions deposited in Ce:LSO crystal, which caused lattice damages and induced colour center in the sample.

The defects and molecular vibration induced by ion irradiation can be investigated by the Raman scattering method [10]. Fig. 5 shows the Raman spectra of the Ce:LSO crystal at the C^{3+} ion irradiated and non-irradiated region over a frequency range of 50–1000 cm^{-1}. The Ce:LSO crystal belong to B-type structure which corresponds to the monoclinic symmetry space group C2/c (C_{2h}^6) with Z = 8 [11]. This structure consists of isolated $[SiO_4]^{4-}$ – tetrahedra. It is shown in group-theory calculations that the vibrational spectrum of free tetrahedral complex $[SiO_4]^{4-}$ correspond to the following relationship:

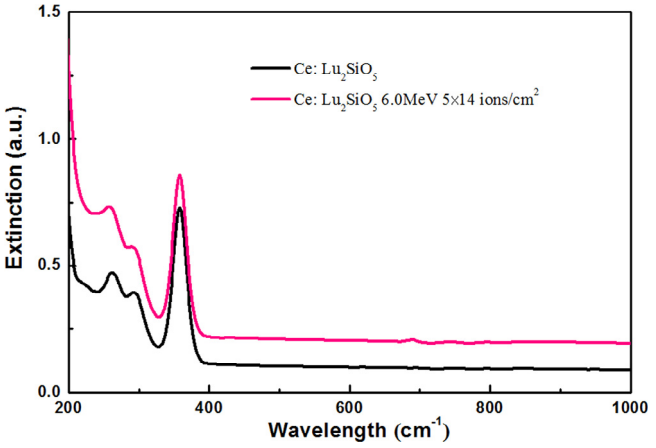

Fig. 4. Optical extinction spectra of a Ce:LSO crystal at wavelengths from 200 to 1000 nm: the black line represents the un-irradiated sample, the pink line represents the sample after application of the 6.0 MeV C^{3+} ions with a fluence 5×10^{14} ions/cm^2. (For interpretation of the references to colour in this figure legend, the reader is referred to the web version of this article.)

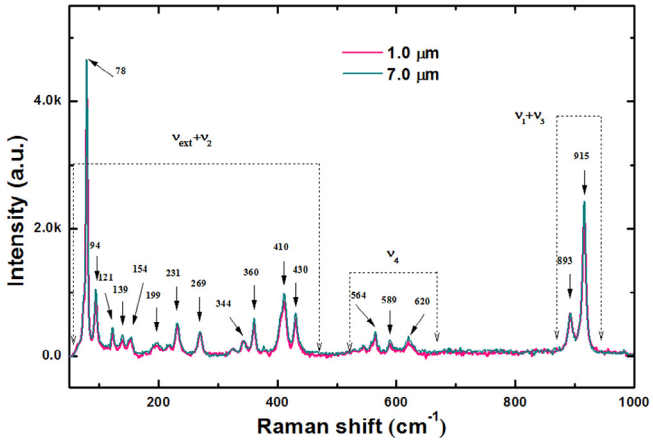

Fig. 5. The Raman spectra of the irradiated and non-irradiated region (1.0 μm and 7.0 μm) by 6.0 MeV C^{3+} ions irradiation with a fluence of 5.0×10^{14} ions/cm^2.

$$\Gamma = A_1(\nu_1) + E(\nu_2) + F_2(\nu_3) + F_2(\nu_4) + F_1(\nu_{f.r}) + F_2(\nu_{tran}) \quad (1)$$

The ν_1–ν_4 vibrations are internal, which can be identified on the basis of experiments and calculations of the vibrational levels of the free $[SiO_4]^{4-}$ anion [12,13]; the free rotation $\nu_{f.r}$ and the translation ν_{tran} vibrations are external oscillations in the crystal unit. The internal and external vibrations modes in the Ce:LSO have been clearly shown in Fig. 5. It is obvious that the spectral properties and lattice vibrations can be influenced by C^{3+} ion irradiation. After C^{3+} ion irradiation, the intensity of the Raman peak is lower than that of the non-irradiated region. Obviously, the damage and deformation induced by C^{3+} ion irradiation result in a decrease in the Raman intensity.

To study the luminescent properties of Ce:LSO after 6.0 MeV C^{3+} ion irradiation with a fluence of 5×10^{14} ions/cm^2, the PL spectra of non-irradiated and irradiated z-cut Ce:LSO crystals were measured and are shown in Fig. 6. In the spectra, the peak at 500 nm is associated with the transitions from the $4f^1$ ground state to the $5d^1$ sublevels of the Ce^{3+} ion, subjected to the crystal field splitting of the host. As shown in Fig. 6, the spectra obtained from the irradiated and non-irradiated samples are similar in sharpness and peak position. This suggests that the average unit cell volume has almost no change. However, compared with a non-irradiated sample, the intensity of the peak at 500 nm is significantly enhanced by approximately 26.8%. Cerium ions substitute for Lu sites with Ce^{3+} and Ce^{4+} in a Ce:LSO host lattice. X-ray

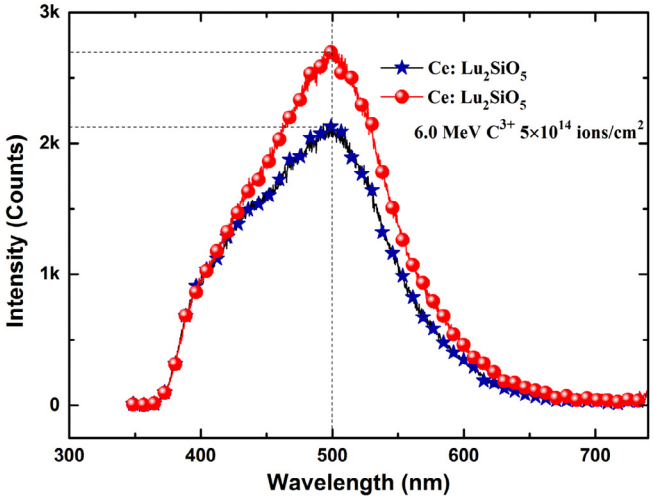

Fig. 6. PL spectra of un-irradiated and irradiated samples (6.0 MeV C^{3+} ion irradiation with a fluence of 5×10^{14} ions/cm^2) at room temperature.

absorption spectroscopy (XAS) results have demonstrated that ions are in two different valence states (Ce^{3+} and Ce^{4+}) [14,15]. We know that the luminescence properties of Ce:LSO are mainly affected by the population of Ce^{3+} because the charge transfer transition in Ce^{4+} is spin-forbidden. If the codopants occupy the interstitial sites near the Ce^{4+} ions, they could serve as donors and supply electrons for Ce^{4+}, leading to an increase in the concentration of Ce^{3+}. Thus, it can be concluded that the population of Ce^{4+} is decreased, meaning the population of Ce^{3+} is improved by 6.0 MeV C^{3+} ion irradiation with a fluence of 5×10^{14} ions/cm^2 [6]. After C^{3+} ion irradiation, we not only manufactured the optical waveguide structure (as shown in Fig. 2), but also greatly enhanced the intensity of the emission peak. Therefore, it is reasonable to deduce that 6.0 MeV C^{3+} ion irradiated Ce:LSO with a fluence of 5×10^{14} ions/cm^2 has potential applications in the waveguides of lasers.

4. Conclusion

The related optical properties before and after C^{3+} ion irradiation of Ce:LSO have been investigated by varied methods. Concerning the optical waveguide properties, the “well + barrier” type waveguide was obtained by 6.0 MeV C^{3+} ions with a fluence of 5×10^{14} ions/cm^2 at room temperature. Additionally, the increased rate of the three absorption bands in the ultraviolet band gradually reduced with the increase of the wavenumber after C^{3+} ion irradiation. It is obvious that the lattice vibrations can be influenced by ion irradiation; we deduced that the mixed stretching/bending mode of the Si-O-Si bridging bond is strengthened by C^{3+} ion irradiation in the Ce:LSO crystal. The photoluminescence investigation reveals that, after C^{3+} ion irradiation, the fluorescence properties were enhanced. We have reason to believe that C^{3+} ion irradiation occupies at the interstitial sites near Ce^{4+} ions, leading to an increased concentration of Ce^{3+} and a great enhancement of the intensity of the emission peak. Therefore, we believe that 6.0 MeV C^{3+} ion irradiated Ce:LSO with a fluence of 5×10^{14} ions/cm^2 has potential applications in the waveguides of lasers.

Acknowledgments

This work is supported by the National Natural Science Foundation of China (No. 11775135), and the State Key Laboratory of Nuclear Physics and Technology at Peking University.

References

[1] J.J. Xie, Y. Shi, L.C. Fan, Z.B. Xu, Opt. Mater. 35 (2013) 744.
[2] M. Kapusta, P. Szupryczynski, C.L. Melcher, M. Moszynski, M. Balcerzyk, A.A. Carey, W. Czarnicki, M.A. Spurrier, A. Syntfeld, IEEE Trans. Nucl. Sci. 2 (2004) 822.
[3] P. Dorenbos, C.W.E. van Eijk, A.J.J. Bos, C.L. Melcher, J. Phys. Condens. Matter 6 (1994) 4167.
[4] L. Jia, M. Gu, X. Liu, S. Huang, B. Liu, C. Ni, IEEE Trans. Nucl. Sci. 57 (2010) 1268.
[5] S. Chen, X. Liu, F. Wu, M. Gu, C. Ni, B. Liu, S. Huang, J. Zhang, Mater. Lett. 100 (2013) 282.
[6] X.L. Liu, F. Wu, S.W. Chen, M. Gu, H. Chen, B. Liu, S.M. Huang, J. Zhang, J. Lumin. 161 (2015) 422.
[7] J.F. Ziegler, Computer code SRIM, http://www.srim.org.
[8] P.J. Chandler, F.L. Lama, Opt. Acta 33 (1986) 127.
[9] D. Yevick, W. Bardyszewiski, Opt. Lett. 17 (1992) 329.
[10] G.A. Baratta, M.M. Arena, G. Strazzulla, L. Colangeli, V. Mennella, E. Bussoletti, Nucl. Instr. Meth. B 116 (1996) 195.
[11] J. Felsche, The crystal chemistry of the rare-earth silicates, Structure and Bonding vol. 13, (1973) 99.
[12] K. Iishi, Am. Mineral. 63 (1978) 1198.
[13] J.L. Servion, B. Piriou, Phys. Status Solidi B 55 (1973) 677.
[14] C.L. Melcher, S. Friedrich, S.P. Cramer, M.A. Spurrier, P. Szupryczynski, R. Nutt, IEEE Trans. Nucl. Sci. 52 (2005) 1809.
[15] C. Mansuy, J.M. Nedelec, R. Mahiou, J. Mater. Chem. 14 (2004) 3274.